

Flux-Bubble Models and Mesonic Molecules

M.M. Boyce, J. Treurniet, and P.J.S. Watson

Ottawa-Carleton Institute for Physics, Carleton University, Ottawa, Ontario, Canada, K1S-5B6

Abstract: It has been shown that the string-flip potential model reproduces most of the bulk properties of nuclear matter, with the exception of nuclear binding. Furthermore, it was postulated that this model with the inclusion of the colour-hyperfine interaction should produce binding. In some recent work a modified version of the string-flip potential model was developed, called the flux-bubble model, which would allow for the addition of perturbative QCD interactions. In attempts to construct a simple $q\bar{q}$ nucleon system using the flux-bubble model (which only included colour-Coulomb interactions) difficulties arise with trying to construct a many-body variational wave function that would take into account the locality of the flux-bubble interactions. In this paper we look at a toy system, a mesonic molecule, in order to understand these difficulties. *En route*, a new variational wave function is proposed that may have a sufficient impact on the old string-flip potential model results that the inclusion of perturbative effects may not be needed.

1. Introduction

For the past 30 years several attempts have been made, with little success, to describe nuclear matter in terms of its constituent quarks. The main difficulty is due to the non-perturbative nature of QCD. The only rigorous method for handling multi-quark systems to date is lattice QCD. However, this is very computationally intensive and given the magnitude of the problem it appears unlikely to be useful in the near future.¹ As a result, more phenomenological

¹ Some very recent advancements have been made in the area of lattice QCD that have reduced computation time by several orders of magnitude. “Now what took hundreds of Cray Supercomputer hours can be done in only a few hours on a laptop computer” [1].

means must be considered.

A good phenomenological model should be able to at least reproduce qualitatively all the overall bulk properties of nuclear matter. In particular,

- nucleon gas at low densities with no van der Waals forces
- nucleon binding at higher densities
- nucleon swelling and saturation of nuclear forces with increasing density
- quark gas at extremely high densities

There are several models that attempt to reproduce these properties but none of them does so completely. In this paper, only the string-flip potential model [2–4], will be considered. This model appears to be promising because it reproduces most of the aforementioned properties with the exception of nucleon binding: instead of producing a binding of about 8 MeV at nuclear density, one finds anti-binding of about 25 MeV. However, various effects have been ignored, such as colour Coulomb and hyperfine forces, relativistic effects and many-quark clusters. In this paper we attempt to understand why, in terms of a toy mesonic molecular system [5].

1.1. The String-Flip Potential Model

The idea of string-flip potential models derives from lattice QCD and meson spectroscopy. A static potential derived from computations in lattice QCD

$$V(r) \sim \sigma r - \frac{4}{3} \frac{\alpha_s}{r} , \quad (1)$$

is confirmed as a phenomenologically satisfactory potential model between quarks and antiquarks by fitting the experimental mesonic spectra. This is basically an interpolation between the long range non-perturbative (σr) and short range perturbative ($-\frac{4}{3} \frac{\alpha_s}{r}$) parts of the force between pairs of quarks (Fig. 1). In the many-body case, the string-flip potential model ignores the short range part of the potential and considers an ensemble of quark-antiquark pairs, $q\bar{q}$, such that the total string length, $\sum r_{q\bar{q}}$, is a minimum: *i.e.*,

$$V = \sigma \sum_{\min\{q\bar{q}\}} r_{q\bar{q}} . \quad (2)$$

This particular model has been used in an attempt to simulate nuclear matter. Although it has an obvious shortcoming, in that it is more applicable to a pion gas, it does surprisingly well at predicting some of the overall bulk properties of nuclear matter [3,4].

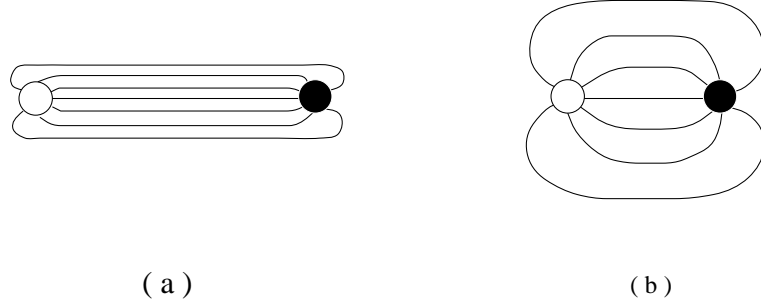


Fig. 1. The colour field lines between quarks collapse upon themselves, due to the self interacting nature of the gluons, to form a flux-tube-like structure. At long distances (a) the fields lines collapse to become almost string-like and at short distances (b) the fields lines expand to become almost QED-like.

In a previous paper, we have extended this simple model to a more realistic one which involves triplets of quarks. Here the flux-tubes leaving each quark meet at a central vertex such that overall length, r , of “flux-tubing” is minimized (*cf.* Fig. 2). The potential energy is simply σr [6]. The effects of this are surprisingly small in going from $SU(2)$ to $SU(3)$: a nucleon gas still forms, and becomes a quark gas above a certain critical density.

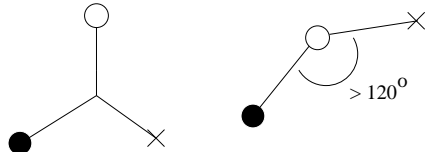


Fig. 2. Flux-tube arrangements for the 3q cluster potentials.

These models are motivated by results from lattice QCD, where variations are taken about minimal lattice field configurations between quarks. We will refer to these, “linear potential models,” as, “ $SU_\ell(N)$ models,” where the $SU(N)$ refers to the $SU_c(N)$ Yang-Mills gauge group and the subscript, “ ℓ ,” refers to, “linear potential,” [2]. In some models each quark has fixed colour to simplify the searches for minimal flux-tube configurations as the system of quarks evolves. When necessary, for clarity, these models will be referred to as, “ $SU'_\ell(N)$ models.”

This paper is divided into four sections: the first discusses the problems faced when attempts are made to extend the string-flip potential model to include perturbative QCD interactions for many-body systems. This is followed by a section on mesonic molecules, where the problems faced with the string-flip potential model and its extensions are examined in detail. In the next we examine a modified wave function, which appears to solve many of the difficulties. The final section reviews all of the findings and their possible consequences for modeling nuclear matter.

2. The Flux-Bubble Model

It appears from earlier work that the String-Flip potential model is incapable of producing nuclear binding without the addition of new interactions [2,7]. However, it turns out to be surprisingly difficult to introduce these into a many-body model. A model was recently proposed, called the Flux-Bubble Model [7], which does allow the perturbative QCD effects to be included.

The primary objective is to construct a model which combines both the non-perturbative (flux-tubes) and perturbative (one-gluon exchange) aspects of QCD in a consistent fashion. In order to simplify this task only colour-Coulomb extensions to a linear potential model using $SU(2)$ colour, *i.e.*, $SU_\ell(2)$, will be considered. The conventional phenomenological potential,

$$V(r) \sim \sigma r - \frac{4}{3} \frac{\alpha_s}{r}, \quad (1)$$

mentioned in § 1.1 does not extend naturally to many-body systems, since the $4/3$ must be replaced by $\lambda_{ij} = -3/4, 1/4$ for unlike and like colours respectively. This gives rise to a Van der Waals potential between colourless nucleons with a $\frac{1}{r^4}$ behaviour. The flux bubble modifies this to

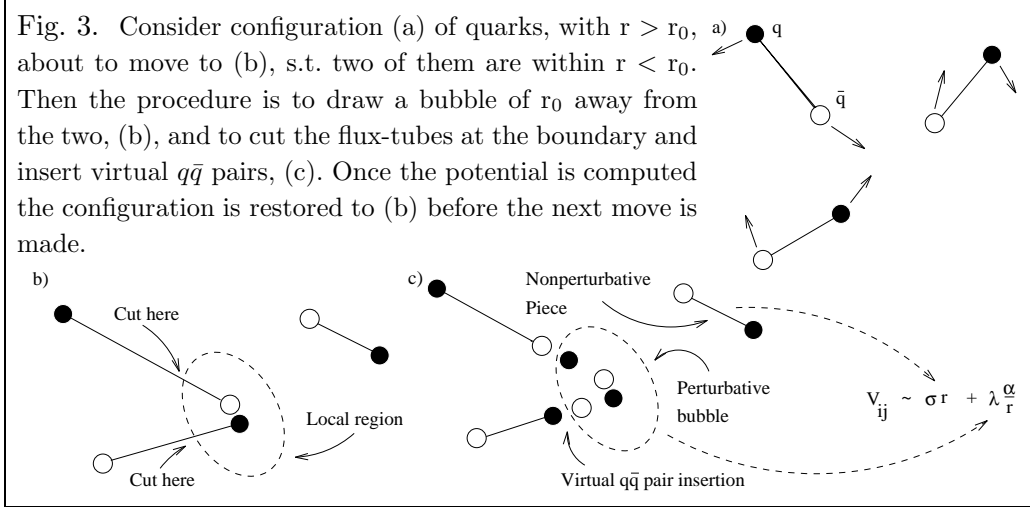
$$v_{ij} \sim \begin{cases} \sigma(r_{ij} - r_0) & \text{if } r_{ij} > r_0 \\ \alpha_s \lambda_{ij} \left(\frac{1}{r_{ij}} - \frac{1}{r_0} \right) & \text{if } r_{ij} < r_0 \end{cases} \quad \begin{array}{c} V \\ \text{---} \\ \text{Linear} \\ \text{Coulomb} \end{array} \quad (3)$$

with $\alpha_s \approx 0.1$. The major difference is that the nonperturbative and perturbative regimes are completely separated in the latter, so that there are no Van Der Waals forces.² When the quarks are separated at a distance greater than r_0 the potential is purely linear and when they are inside this radius it is purely Coulomb. In effect, for distances less than r_0 , a “bubble” is formed in which the quarks are free to move around, in an asymptotically free fashion. In both distance regimes the net colour of the system is neutral, and phenomenologically the models are almost identical for a single $q\bar{q}$ system.

This extension of the linear potential, although simple for a pair of quarks, becomes more complex when considering many pairs of quarks. In particular, it is difficult to construct a potential model when some set of quarks lie within r_0 , without forming a colour singlet so that they must be connected to more distant quarks by flux-tubes. An *ansatz* that satisfies these requirements is obtained by inserting virtual $q\bar{q}$ pairs across any of the intersection boundaries

² We have also considered a “smoothed” potential where the Coulomb term has an exponential cutoff of the form $e^{-\frac{r}{r_0}}$, and the linear term is turned on by a similar function. This makes a negligible difference to our results.

formed by the flux-tubes with the bubbles. Now the segments of flux-tubes that lie outside the bubbles remain intact while the segments inside simply dissolve. Fig. 3 illustrates the dynamics of this model.



Note the insertion of the virtual $q\bar{q}$ pairs allows the construction of colourless objects. These are solely used as a tool to calculate the overall length of the flux-tube correctly, and not used in computing the Coulomb term however, as the field energy is already taken into account by the “real” quarks inside the bubbles. In general, once the bubbles have been determined, the flux-tubes must be reconfigured in order to minimize the linear part of the potential. Although the model is currently for $SU_\ell(2)$ it would be straightforward to extend it to a full $SU_\ell(3)$ model with all the one-gluon exchange phenomena.

In the previous case for the $SU_\ell'(3)$ model, given in ref. [2], we adopted a wave function with two “independent” parameters, ρ (density) and β (inverse correlation length); *i.e.*,

$$\Psi_{\alpha\beta} = \underbrace{e^{-\sum_{\min\{q\bar{q}\}} (\beta r_{q\bar{q}})^\alpha}}_{\text{Correlation} \Leftrightarrow \beta} \underbrace{\prod_{\text{colour}} |\Phi(r_{p_k})|}_{\text{Slater} \Leftrightarrow \rho}, \quad (4)$$

where α was fixed.³ We were able to use a scaling trick to reduce the number of variation degrees of freedom to one, since ρ and β varied parametrically with a single parameter, θ , as

$$(\beta, \rho^{1/3}) \longrightarrow \zeta(\theta) (\cos \theta, \sin \theta) \quad (5)$$

where $[\zeta(\theta)] \sim fm^{-1}$. However, for the flux-bubble potential, this scaling

³ Here, $\alpha \approx 1.75$, and $\alpha = 2$ gives the harmonic oscillator case.

transformation is broken. This extra degree of freedom greatly increases the computation time, since we must now perform a 2-dimensional minimization.

We have, however, been able to show that the results of the computation are qualitatively similar to previous results [7]: in other words, the flux bubble does not give rise to additional binding. However, to obtain satisfactory results requires a coarse 10×10 mesh of points, in ρ and β , and hence 18hrs of CPU time on an 8 node farm. Clearly this procedure would be ridiculously slow if more parameters were to be added. Thus a rapid method of checking different wave functions, minimization procedures and various aspects of the string-flip and flux-bubble potential models is desirable.

3. Mesonic Molecules

A possible mini-laboratory is a mesonic-molecule [8], Q_2 , consisting of two heavy quarks and two relatively light antiquarks: see Fig. 4. The quarks are assumed to be heavy so that the light antiquarks can move around freely without disturbing their positions: *i.e.*, the Born-Oppenheimer approximation is valid. By varying the distance, R , between the heavy quarks a mesonic-molecular potential, $U(R)$, can be computed.

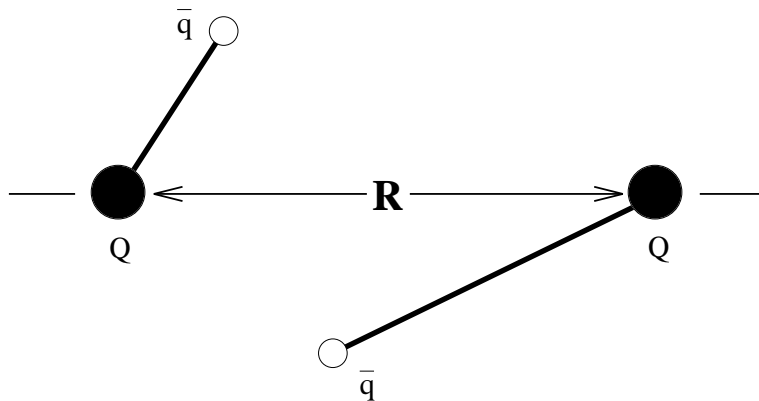


Fig. 4. A mesonic-molecule, Q_2 , with two heavy quarks and two light antiquarks.

The Schrödinger equation that describes the effective potential, $U(R)$, is given by [9]

$$\left(\frac{1}{2m_q} \sum_{\bar{q}} \vec{\nabla}_{\bar{q}}^2 + V \right) \Psi = U(R) \Psi ; \quad (6)$$

we shall assume $m_q \approx 330 \text{ MeV}$. The potential V describes the many-body nature of the four quark system, and is therefore model dependent. This equation can be solved variationally for $\bar{U}(R)$, at fixed values of R , by guessing at

the form of the wave function, Ψ , and minimizing

$$\bar{U} = \bar{T} + \bar{V} \quad (7)$$

with respect to the parameters in Ψ .

The expectation values \bar{T} and \bar{V} are found by using the Metropolis algorithm [2,10], and the optimal parameters for Ψ are found by using the distributed minimization algorithm [5,11] on $\bar{U}(R)$. This was developed to handle the problem of reducing CPU overhead. It involves the usage of several *CPU*'s to perform interlaced parabolic searches for the minima of a given surface. For the Q_2 system this algorithm yields

$$\tau_{\text{CPU}} \sim \mathcal{O}\left(\frac{p}{m}\right), \quad (8)$$

for p parameters and m computers: similar results are expected for nuclear matter calculations.

The Q_2 system provides a good way of checking potential models for the possibility of nuclear (mesonic) binding. Because of its simplicity, it allows for investigating various wave functions and minimization schemes with minimal computational effort.

A final useful feature is that the integration can be reduced to a 4-D one if Coulomb interactions are ignored, and a 5-D one if they are included. This allows us to avoid the Metropolis procedure entirely, and use multi-dimensional Gaussian methods, which we use a check on the Monte-Carlo methods

3.1. Sensitivity to the Variational Parameters

When the $SU_\ell(2)$ string-flip potential model was investigated in ref. [4] the parameter α in the variational wave function, given by Eq. 4, was fixed by requiring that it minimize the total energy at zero density. Since this could be done analytically it allowed for a reduction in the number of variational parameters used in the Monte Carlo. It was assumed that constraining α would have very little effect on the physics as a function of density since the results only vary by about 1% for $1.5 < \alpha < 2.1$ at zero density. The validity of this claim can now be checked more thoroughly by using the Q_2 mini-laboratory.

Fig. 5 shows a plot of the Monte Carlo results, obtained *via* Eqs. 7, 9, and 10, for $\bar{U}(R)$ where α is allowed to vary, $\alpha = 2.00$, and $\alpha = 1.74$. The $\alpha = 2.00$ value was used in the old $SU_\ell(2)$ model [4], and $\alpha \approx 1.74$ was the value that minimized $\bar{U}(R)$ at infinite separation. The values of $\bar{U}(R)$ at the end points of the curves, from $R = 0 \text{ fm}$ and out to $R = 5 \text{ fm}$, were checked against the analytic solution given by Eq. A.8.

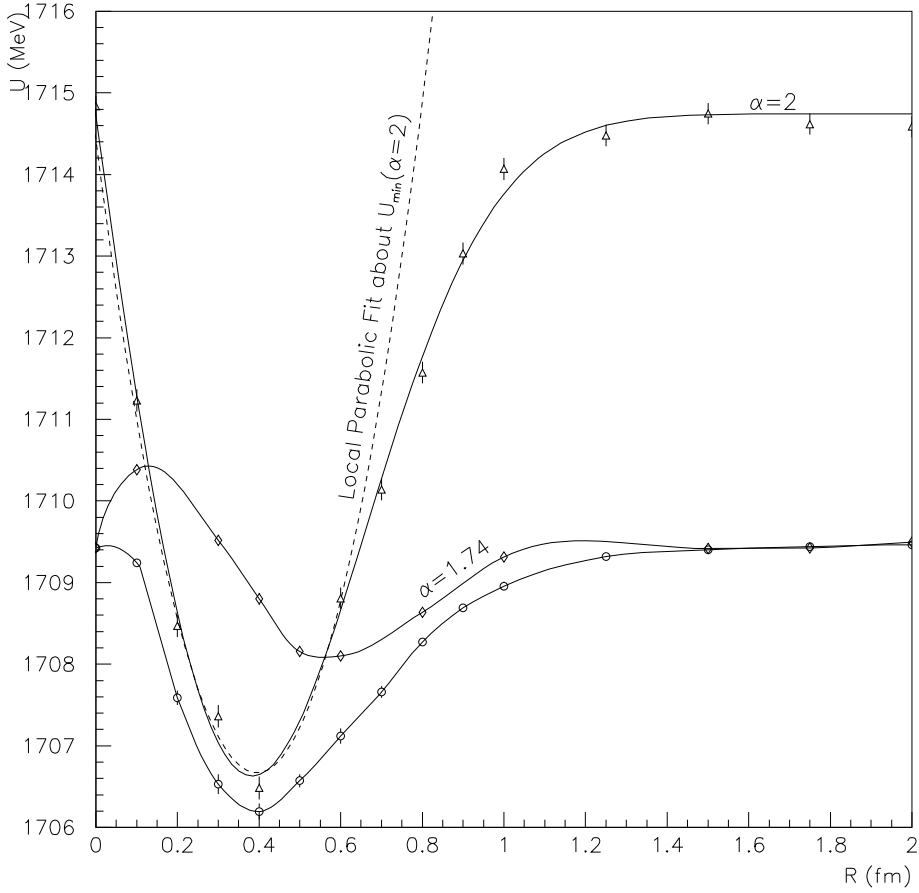


Fig. 5. $\bar{U}(R)$ where α is allowed to vary, fixed at 2, and fixed at 1.74.

We find that when α is allowed to vary, α and β become highly correlated. Regardless, looking at the maximum fluctuations about the central values of the parameters α , β , and $\bar{U}(R)$ we have [5] $\alpha \approx (1.88 \pm 0.13)$, $\beta \approx (1.32 \pm 0.05) \text{ fm}$, and $\bar{U}(R) \approx (1710 \pm 4) \text{ MeV}$, which is certainly less than a 1% effect in the total energy [4]. However the relative energy $U(R) - U(\infty)$ depends critically on the variational procedure.

Surprisingly $\bar{U}(R)|_{\alpha=2}$ gives a much deeper well than if α was left as a free parameter: *i.e.*, $D \approx \mathcal{O}(8) \text{ MeV}$ [5]. For certain fixed values of α , for example $\alpha \approx 1.74$ in Fig. 5, the potential gives a slight short range repulsion, which becomes quite dramatic for $\alpha \approx 1.0$. This is, of course, totally unphysical, since $U(R) - U(\infty) \leq 0$. We conclude from this that it is unsafe to fix α , since the well depth can vary by nearly a factor of 3. However, it is fairly safe to assume that the results of past papers [4,2] will not change significantly if α is allowed to vary. For the rest of the paper, we consider simultaneous minimizations of α and β .

3.2. A General Survey of Extensions to $SU_\ell(2)$

In this section the effects of extending the old $SU_\ell(2)$ [4] model to include flux-bubbles, with and without fixed colour (*i.e.*, $SU_\ell(2)$ and $SU'_\ell(2)$ respectively), will be investigated in the context of the mesonic-molecular system, Q_2 . For the old $SU_\ell(2)$ model the variational wave function was assumed to be of the form [4],

$$\Psi_{\alpha\beta} = e^{-\sum_{\min\{Q\bar{q}\}} (\beta r_{Q\bar{q}})^\alpha}, \quad (9)$$

where α and β are variational parameters, and $r_{Q\bar{q}}$ is the distance between a given $Q\bar{q}$ pair. The summation in the exponent of the wave function is over the set of $Q\bar{q}$ pairs that requires the least amount of flux-tubing: *i.e.*,

$$V = \sigma \sum_{\min\{Q\bar{q}\}} r_{Q\bar{q}} \equiv \sigma \min\{\sum_{\{Q\bar{q}\}} r_{Q\bar{q}}\}, \quad (10)$$

or more explicitly

$$V = \sigma \min\{r_{Q_1\bar{q}_1} + r_{Q_2\bar{q}_2}, r_{Q_1\bar{q}_2} + r_{Q_2\bar{q}_1}\}, \quad (11)$$

cf. Eq. (2). Therefore, the kinetic energy is simply

$$\bar{T} = \frac{\alpha\beta^\alpha}{2m_q} \left\langle \sum_{\min\{Q\bar{q}\}} [\alpha(1 - (\beta r_{Q\bar{q}})^\alpha) + 1] r_{Q\bar{q}}^{\alpha-2} \right\rangle. \quad (12)$$

Now, if we assume for the moment that the colour is affixed to the quarks (*i.e.*, $SU'_\ell(2)$), then the most general flux-bubble potential is of the form

$$V = \sigma \sum_{\min\{Q\bar{q}\}} (r_{Q\bar{q}} - r_0) \theta(r_{Q\bar{q}} - r_0) + \alpha_s \sum_{i < j} \lambda_{p_ip_j} \left(\frac{1}{r_{p_ip_j}} - \frac{1}{r_0} \right) \theta(r_0 - r_{p_ip_j}), \quad (13)$$

with particle index $p_k \in \{Q_i, \bar{q}_j | i, j = 1, 2\}$, such that $k = 1, 2, 3, 4$, and $SU_c(2)$ colour factor

$$\lambda_{p_ip_j} = \begin{cases} -\frac{3}{4} & \text{if } p_ip_j \in \{\bar{q}Q\} \\ \frac{1}{4} & \text{if } p_ip_j \in \{\bar{q}\bar{q}, QQQ\} \end{cases}. \quad (14)$$

This potential can be rewritten into the more enlightening form

$$\begin{aligned} V = & \sum_{\min\{q_i\bar{q}_j\}} \left[\sigma (r_{q_i\bar{q}_j} - r_0) \theta(r_{q_i\bar{q}_j} - r_0) - \frac{3}{4} \alpha_s \left(\frac{1}{r_{q_i\bar{q}_j}} - \frac{1}{r_0} \right) \theta(r_0 - r_{q_i\bar{q}_j}) \right] \\ & - \frac{3}{4} \alpha_s \sum_{q_i\bar{q}_j \in \min\{q_i\bar{q}_j\}_+} \left(\frac{1}{r_{q_i\bar{q}_j}} - \frac{1}{r_0} \right) \theta(r_0 - r_{q_i\bar{q}_j}) \end{aligned}$$

$$+ \frac{1}{4} \alpha_s \sum_{q_i q_j \in \min\{q_i \bar{q}_j\}_-} \left(\frac{1}{r_{q_i q_j}} - \frac{1}{r_0} \right) \theta(r_0 - r_{q_i q_j}), \quad (15)$$

where $q_i \in \{Q, q\}$. The sets $\overline{\min\{q_i \bar{q}_j\}}_+$ and $\overline{\min\{q_i \bar{q}_j\}}_-$ contain the attractive and repulsive quark pairings, respectively, in the complement ($\overline{\min\{q_i \bar{q}_j\}}$) of the set $\min\{q_i \bar{q}_j\}$: *i.e.*,

$$\overline{\min\{q_i \bar{q}_j\}} = \overline{\min\{q_i \bar{q}_j\}}_+ \cup \overline{\min\{q_i \bar{q}_j\}}_-.$$

The two terms inside the square brackets of Eq. 15 represents a linear potential followed by its colour-Coulomb extension: *cf.* Eq. (1). The remaining terms represent the rest of the colour-Coulomb interactions, which contain both attractive and repulsive bits.

Fig. 6 shows the results of the Monte Carlo for the linear potential and its various variants, including the flux-bubble potential.

We have also considered relativistic effects, via the relativistic Dirac-Hartree-Fock method(*e.g.*, [18]), assuming the flux-tube interaction is a Lorentz scalar.

$$\sum_{\min\{Q \bar{q}\}} [\nabla_{\bar{q}}^2 + (m_q + \sigma r_{Q \bar{q}})^2] \Psi = U^2(R) \Psi. \quad (16)$$

This slightly exacerbates the problem, in that the potential becomes even more shallow. We note in passing that it is not possible to solve the physically interesting case of massless quarks interacting via a Coulomb potential in addition to the linear term, since it introduces an effective $1/r^2$ potential in Eq. (16).

To compare these potentials with more conventional methods, we would like to investigate whether they can bind heavy quarks into molecular systems, and to what extent they resemble conventional inter-nucleon potentials. The details of this analysis can be found in appendix A. A reduced heavy quark mass of

$$\mu_Q \gtrsim (53.7 \pm 1.9) \text{ GeV} \quad (17)$$

is required to obtain binding for these potentials. This should not be too surprising as the potential wells are very shallow,

$$\bar{D} \approx (2.986 \pm 0.030) \text{ MeV}. \quad (18)$$

To find whether the string-flip potential models actually mimic pion exchange, the asymptotic parts of the $\bar{U}(R)$'s are fitted to a Yukawa potential. The results

⁴ *e.g.*, if $\min\{q_i \bar{q}_j\} = \{Q_1 \bar{q}_2, Q_2 \bar{q}_1\}$ then $\overline{\min\{q_i \bar{q}_j\}} = \{Q_1 \bar{q}_1, Q_2 \bar{q}_2, Q_1 Q_2, \bar{q}_1 \bar{q}_2\}$, which implies $\overline{\min\{q_i \bar{q}_j\}}_+ = \{Q_1 \bar{q}_1, Q_2 \bar{q}_2\}$ and $\overline{\min\{q_i \bar{q}_j\}}_- = \{Q_1 Q_2, \bar{q}_1 \bar{q}_2\}$.

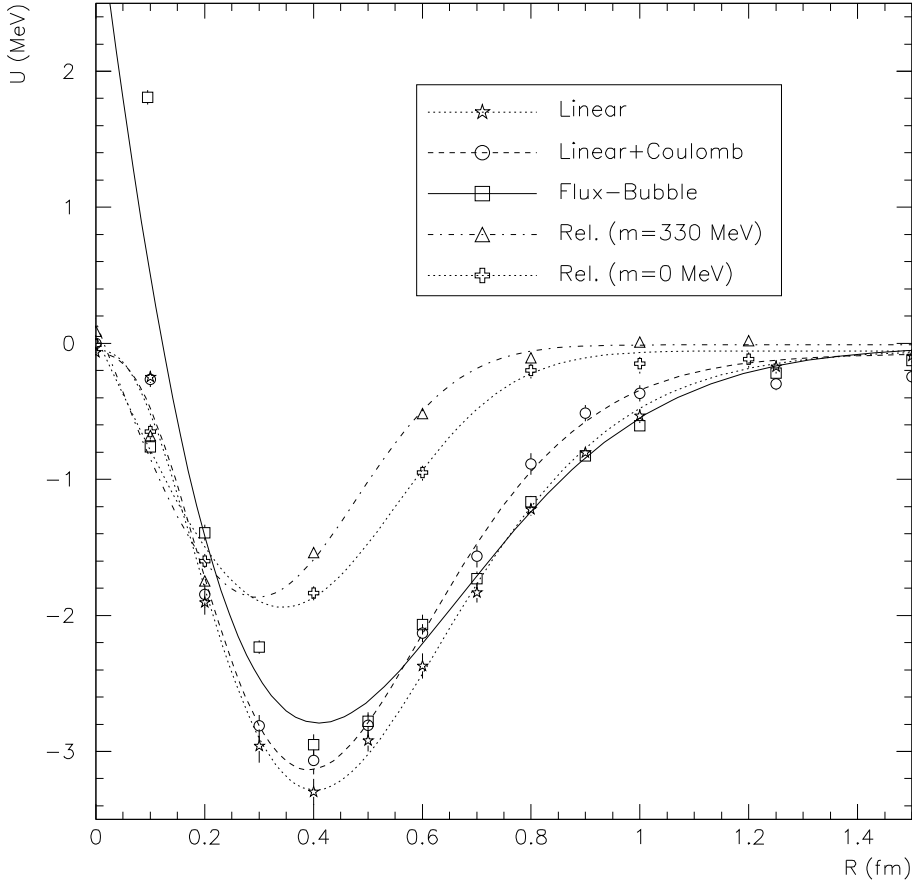


Fig. 6. The binding energy, $E_B(R)$ ($= U(R) - U_\infty$ s.t. $U_\infty \equiv U(\infty)$), for the Q_2 system as function of heavy quark separation for a linear (Eq. (10)), a linear-plus-Coulomb (square brackets of Eq. (15)), and a flux-bubble (Eq. (15)) potential model. Also included, for contrast, are the semi-relativistic results discussed in § 5. The curves in these plots have been parameterized by $u(r) \sim u_0 \{e^{-2\kappa b(r-r_0)^\alpha} - 2\kappa e^{-b(r-r_0)^\alpha}\} (r-\varepsilon)^\eta$ (cf. Morse potential [9,12]).

of the analysis yielded an effective exchange mass of

$$\bar{m}_{\text{ex}} \approx (636 \pm 41) \text{ MeV}, \quad (19)$$

which is about 4.5 times too big, so the potential is much too short-range.

Finally, the flux-bubble potential is extended to allow the colour to move around. The potential is similar to that of Eq. 15 except now the particle indices, p_k , carry colour degrees of freedom:

$$q_k \in \{R_i, \bar{B}_i, r_i, \bar{b}_i | i = 1, 2\} \subseteq SU_c(2),$$

$$\bar{q}_k \in \{\bar{R}_i, B_i, \bar{r}_i, b_i | i = 1, 2\} \subseteq \overline{SU_c(2)},$$

i.e.,

$$b \sim \bar{r}, \dots, \text{etc.} \Leftrightarrow SU_c(2) \sim \overline{SU_c(2)},$$

where the capital case letters represent the heavy quarks, the lower case letters represent the light quarks, the letters r and R represent the red quarks, and the letters b and B represent the blue quarks. Therefore, the $\min\{Q\bar{q}\}$ in Eq. 15 is determined by Eq. 10 such that colour is no longer fixed to a given quark. Fig. 7 shows the results of the Monte Carlo for this potential.

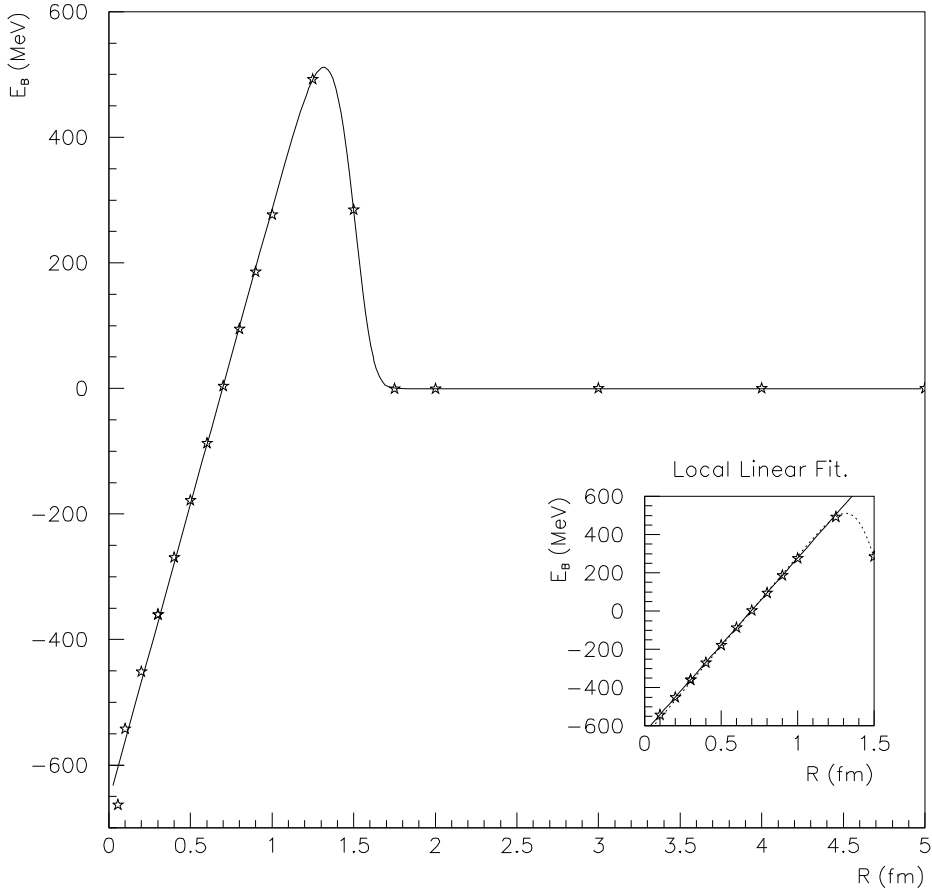


Fig. 7. The Q_2 binding energy curve using the full flux-bubble interaction, *i.e.*, in which the colour is allowed to move around. This curve was parameterized using $u(r)$ given in Fig. 6.

Obviously the result of this is totally different from the fixed colour model. For $R \leq 1 \text{ fm}$, the potential just reproduces the potential between the heavy quarks: a linear fit to this region (see the insert in Fig. 7) yields a slope of $(909.8 \pm 1.0) \text{ MeV/fm}$! Near the origin the potential behaves as $-\frac{1}{r}$, which is due to the Coulomb attraction between the two heavy quarks. Beyond

$R = 1 \text{ fm}$ there is a barrier and beyond this no more structure. This apparently bizarre result can be understood as follows: if two mesons, each containing a heavy quark and a light anti-quark, are brought together from infinity they initially feel a repulsive force. However, it then becomes energetically preferable for the two mesons to dissociate into one meson containing two heavy quarks and another containing two light anti-quarks. This arises since the model has a Pauli-Gursey symmetry [14]: quarks and antiquarks have the same representations. Although potentially realistic as a description of meson-anti-meson interaction, the $SU_c(2)$ with moving colour does not make a satisfactory model for nuclear matter.

From this discussion, it is clear that the extensions to the string-flip potential model to include the colour-Coulomb interactions have essentially no effect on the Q_2 potential, and certainly will not give rise to nuclear binding. Furthermore, the string-flip potential does not give a long-range interaction similar to pion exchange. When the colour was allowed to move around a highly unphysical situation occurs which suggested that there was perhaps a problem with using $SU_c(2)$ or with the variational wave function itself — perhaps even both. In the next section we investigate an alternative wave-function.

4. A New Wave Function

The two previous sections have shown that modifying the potential or modifying the variational procedure produces a relatively small effect on the Q_2 interaction. It therefore seems plausible that the fundamental problem lies in our choice of the wave-function. A hint is to note the similarity between the Q_2 mesonic-molecular system and H_2 molecular system. The key reason for the molecular binding is the screening effect caused by the electrons which are for the most part localized in between the protons. This localization is achieved by using a variational wave function that is a superposition of the direct product of two ground state hydrogen atoms, [9,13,15]

$$\Psi \sim e^{-\beta(r_{e_1 P_1} + r_{e_2 P_2})} + e^{-\beta(r_{e_2 P_1} + r_{e_1 P_2})}. \quad (20)$$

The effect is that of a “bond-centred” wave function. Although the Q_2 system is far removed from its H_2 cousin from a dynamical point of view and the motivations for achieving localization are quite different, it would seem plausible to use a similar *ansatz*:

$$\Psi_{\alpha,\beta} = e^{-\beta^\alpha(r_{\bar{q}_1 Q_1}^\alpha + r_{\bar{q}_2 Q_2}^\alpha)} + e^{-\beta^\alpha(r_{\bar{q}_2 Q_1}^\alpha + r_{\bar{q}_1 Q_2}^\alpha)}. \quad (21)$$

If $\bar{q}_1 Q_1$ and $\bar{q}_2 Q_2$ represent two separate mesons then the first term represents the internal meson interactions while the second term represents the exter-

nal meson interactions. Notice that the external interactions shut off as the separation, R , between the two heavy quarks becomes large,

$$\lim_{R \rightarrow \infty} \bar{\Psi}(R) = e^{-\beta^\alpha(r_{\bar{q}_1 Q_1}^\alpha + r_{\bar{q}_2 Q_2}^\alpha)} \quad (22)$$

which is the desired property. Furthermore, when the light quarks are close in space, $\Psi(R)$ is considerably enhanced.

Using Eq. 6 and Eq. 22 the kinetic energy contribution is more complex for this wave-function, and now becomes [2,5,16]

$$\bar{T} = 2\bar{T}_{-s} - \bar{F}^2, \quad (23)$$

where

$$\begin{aligned} \bar{T}_{-s} &= \frac{-1}{4m_q} \sum_{\bar{q}} \langle \nabla_{\bar{q}}^2 \ln \Psi \rangle \\ &= \frac{\alpha \beta^\alpha}{4m_q} \left\langle \frac{(\alpha+1)}{\Psi} \left[(r_{\bar{q}_1 Q_1}^{\alpha-2} + r_{\bar{q}_2 Q_2}^{\alpha-2}) e^{-\beta^\alpha(r_{\bar{q}_1 Q_1}^\alpha + r_{\bar{q}_2 Q_2}^\alpha)} \right. \right. \\ &\quad \left. \left. + (r_{\bar{q}_2 Q_1}^{\alpha-2} + r_{\bar{q}_1 Q_2}^{\alpha-2}) e^{-\beta^\alpha(r_{\bar{q}_2 Q_1}^\alpha + r_{\bar{q}_1 Q_2}^\alpha)} \right] \right. \\ &\quad \left. + \frac{\alpha \beta^\alpha}{\Psi^2} [(r_{\bar{q}_1 Q_1}^2 + r_{\bar{q}_1 Q_2}^2 - R^2) r_{\bar{q}_1 Q_1}^{\alpha-2} r_{\bar{q}_1 Q_2}^{\alpha-2} \right. \\ &\quad \left. + (r_{\bar{q}_2 Q_1}^2 + r_{\bar{q}_2 Q_2}^2 - R^2) r_{\bar{q}_2 Q_1}^{\alpha-2} r_{\bar{q}_2 Q_2}^{\alpha-2} \right. \\ &\quad \left. - (r_{\bar{q}_1 Q_1}^{2\alpha-2} + r_{\bar{q}_2 Q_2}^{2\alpha-2} + r_{\bar{q}_2 Q_1}^{2\alpha-2} + r_{\bar{q}_1 Q_2}^{2\alpha-2})] \right. \\ &\quad \left. \times e^{-\beta^\alpha(r_{\bar{q}_1 Q_1}^\alpha + r_{\bar{q}_2 Q_1}^\alpha + r_{\bar{q}_1 Q_2}^\alpha + r_{\bar{q}_2 Q_2}^\alpha)} \right\rangle, \end{aligned} \quad (24)$$

and

$$\begin{aligned} \bar{F}^2 &= \frac{1}{2m_q} \sum_{\bar{q}} \langle (\nabla_{\bar{q}} \ln \Psi)^2 \rangle \\ &= \frac{\alpha^2 \beta^{2\alpha}}{2m_q} \left\langle \frac{1}{\Psi^2} \left[(r_{\bar{q}_1 Q_1}^{2\alpha-2} + r_{\bar{q}_2 Q_2}^{2\alpha-2}) e^{-2\beta^\alpha(r_{\bar{q}_1 Q_1}^\alpha + r_{\bar{q}_2 Q_2}^\alpha)} \right. \right. \\ &\quad \left. \left. + (r_{\bar{q}_2 Q_1}^{2\alpha-2} + r_{\bar{q}_1 Q_2}^{2\alpha-2}) e^{-2\beta^\alpha(r_{\bar{q}_2 Q_1}^\alpha + r_{\bar{q}_1 Q_2}^\alpha)} \right] \right. \\ &\quad \left. + [(r_{\bar{q}_1 Q_1}^2 + r_{\bar{q}_1 Q_2}^2 - R^2) r_{\bar{q}_1 Q_1}^{\alpha-2} r_{\bar{q}_1 Q_2}^{\alpha-2} \right. \\ &\quad \left. + (r_{\bar{q}_2 Q_1}^2 + r_{\bar{q}_2 Q_2}^2 - R^2) r_{\bar{q}_2 Q_1}^{\alpha-2} r_{\bar{q}_2 Q_2}^{\alpha-2} \right] \right\rangle \end{aligned}$$

$$\begin{aligned}
& + (r_{\bar{q}_2 Q_1}^2 + r_{\bar{q}_2 Q_2}^2 - R^2) r_{\bar{q}_2 Q_1}^{\alpha-2} r_{\bar{q}_2 Q_2}^{\alpha-2}] \\
& \times e^{-\beta^\alpha (r_{\bar{q}_1 Q_1}^\alpha + r_{\bar{q}_2 Q_1}^\alpha + r_{\bar{q}_1 Q_2}^\alpha + r_{\bar{q}_2 Q_2}^\alpha)} \Bigg\} . \tag{25}
\end{aligned}$$

It serves as a good check of the computation that in the large R limit the kinetic energy reduces to the kinetic energy for the old wave function in the same limit:

$$\begin{aligned}
\lim_{R \rightarrow \infty} \bar{T}(R) &= \frac{\alpha \beta^\alpha}{2m_q} \left\langle (\alpha + 1) (r_{\bar{q}_1 Q_1}^{\alpha-2} + r_{\bar{q}_2 Q_2}^{\alpha-2}) - \alpha \beta^\alpha (r_{\bar{q}_1 Q_1}^{2\alpha-2} + r_{\bar{q}_2 Q_2}^{2\alpha-2}) \right\rangle \\
&= \frac{\alpha \beta^\alpha}{2m_q} \left\langle \sum_{i=1}^2 [\alpha(1 - (\beta r_{\bar{q}_i Q_i})^\alpha) + 1] r_{\bar{q}_i Q_i}^{\alpha-2} \right\rangle , \tag{26}
\end{aligned}$$

cf. Eq. 12. Also direct evaluation of the RHS leads to (assuming Ψ is properly normalized)

$$\lim_{R \rightarrow \infty} \bar{T}(R) = \frac{g_T(\alpha)}{m_q} \beta^2 , \tag{27}$$

which is just the kinetic term for the analytic solution given by Eq. A.1.

The Monte Carlo computations that were done, using the pseudo-hydrogen wave function, $\tilde{\Psi}_H$ (*i.e.*, Eq. 9) in § 3.2, have been repeated here for the pseudo-hydrogen-molecular wave function, $\tilde{\Psi}_{H_2}$ (*i.e.*, Eq. 21), and are shown in Figs. 8 and 9.

It can be immediately seen, that there is a dramatic contrast between the figures for $\tilde{\Psi}_H$ and $\tilde{\Psi}_{H_2}$. The depth of the pseudo-Morse potential has increased from around 5 MeV to around 80 MeV. This is sufficient to bind quark molecules. From the plots in Fig. 8 we find that heavy quarks with

$$\mu_Q \gtrsim (660 \pm 24) \text{ MeV} . \tag{28}$$

such as c and b would form bound quark molecules. We can fit a Yukawa potential to the tail of the potential to give an effective Yukawa mass

$$\bar{m}_{\text{ex}} \approx (575 \pm 32) \text{ MeV} , \tag{29}$$

via table A.3, which is still high compared to the pion mass. Also included in Fig 8, are plots for α fixed at 2 and 1.74. The subtle effects seen with the old wave function are simply overwhelmed by the depth of the potential: in fact, all of the curves are independent of the details of the potential. Therefore, any new model of nuclear matter that incorporates $\tilde{\Psi}_{H_2}$ should run into no difficulties by fixing α .

The final figure, Fig. 9, of the flux-bubble model with moving colour is quite intriguing. The anomalies in Fig. 7 have disappeared; the light quarks have

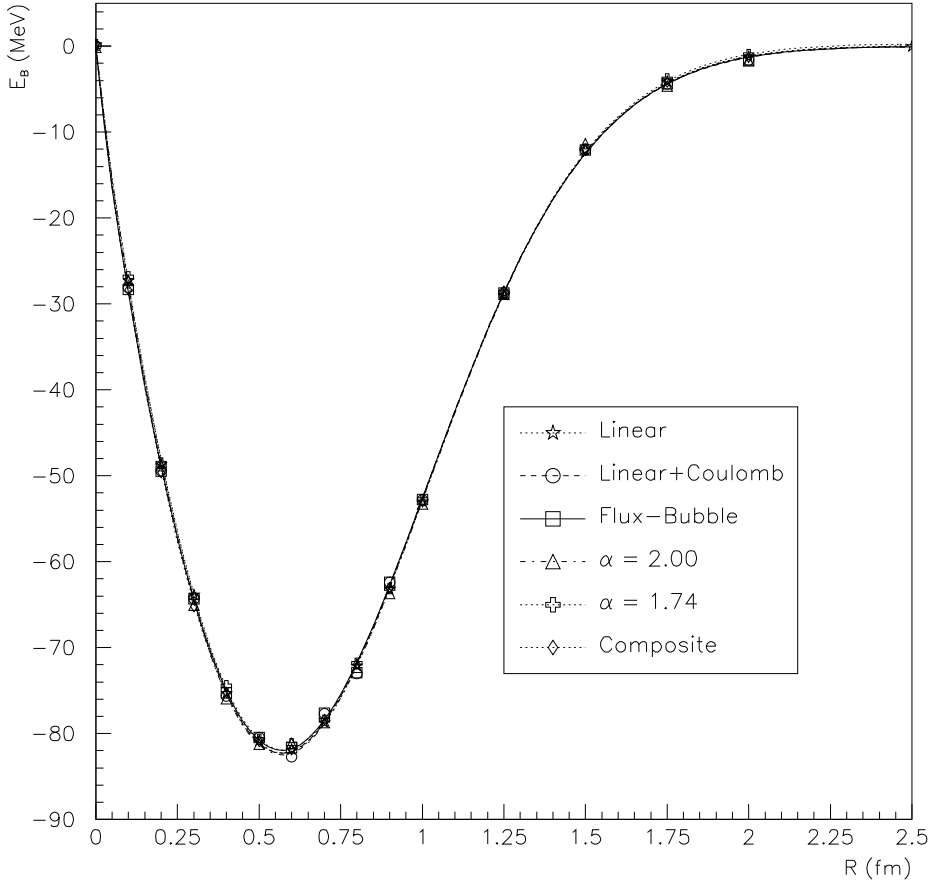


Fig. 8. The binding energy, $E_B(R)$, for the Q_2 system as function of heavy quark separation for a linear, a linear-plus-Coulomb, and a flux-bubble potential model. Also shown, are the curves for $\alpha = 2.00$ and 1.74 , and the composite model discussed in § 5. The curves in these plots have been parameterized by $u(r)$ given in Fig 6.

not drifted away as an isolated pair to leave a linear potential between the heavy quarks. Naïvely, this seems to suggest that the problem was with the wave function and not $SU_c(2)$. However, this is not quite the case, since the old wave function gives an interior well depth which is twice as deep. Therefore, it is still energetically more preferable for the Q_2 system to dissociate into two isolated mesons; one with two light quarks and the other with two heavy ones. The interior of the well can be fitted to a Coulomb potential of the form,

$$V_C(r) = -\frac{a}{r} \left(1 - e^{-\beta r}\right) + V_\infty \quad (30)$$

(see insert in Fig. 9), with $a \approx (135.5 \pm 2.9) \text{ MeV fm}$, $\beta \approx (2.844 \pm 0.048) \text{ fm}^{-1}$, $V_\infty \approx (68.3 \pm 2.6) \text{ MeV}$. The term in the brackets is included to mimic

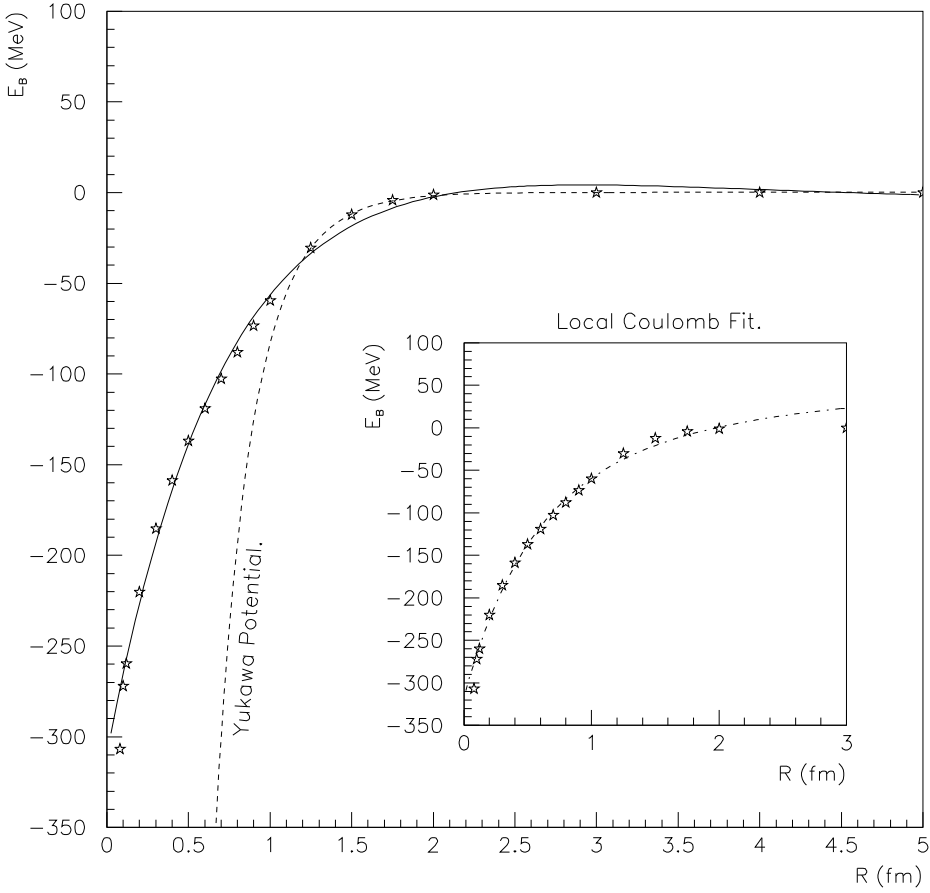


Fig. 9. The Q_2 binding energy curve using the full flux-bubble interaction, *i.e.*, in which the colour is allowed to move around. This curve was parameterized using $u(r)$ given in Fig. 6.

the overlap between the charge distributions of two mesonic systems. In terms of α_s , the hyperfine constant for this region of the potential is

$$\alpha_{Q_2} \approx (6.86 \pm 0.15)\alpha_s. \quad (31)$$

The interior part of the potential is quite deep and bottoms out at $\mathcal{O}(-270)$ MeV, at which point the $-\alpha_s/r$ term for the heavy quarks kicks in (*i.e.*, for $R \leq 0.1$ fm). The exterior part of the potential fits to a Yukawa potential with $m_{\text{ex}} \approx (612 \pm 32)$ MeV (*via* table A.3).

5. Discussion

Various aspects of model building for nuclear matter have been examined in the context of the Q_2 system. The ramifications of these investigations will now be discussed. The most important result is the new variational wave function, Eq. 21. This new wave function makes a massive change in the depth of the Q_2 potential well, increasing it by a factor of 27, which is deep enough to bind relatively light quarks: *i.e.*, $m_q \gtrsim \mathcal{O}(m_s)$. The wave function also fulfills the requirement of handling local flux-bubble interactions, which becomes apparent when looking at the “before” and “after” pictures (of moving colour) in Figs. 7 and 9, respectively. Therefore, in $SU_\ell(2)$ for a many quark system this would suggest the following *ansatz*:

$$\Psi \sim \text{Perm} |\tilde{\Psi}_H(r_{p_i p_j})| \prod_{\text{colour}} |\Phi(r_{p_k})| \quad (32)$$

where

$$\tilde{\Psi}_H(r_{p_i p_j}) = e^{-(\beta r_{p_i p_j})^\alpha}, \quad (33)$$

$\text{Perm} |\tilde{\Psi}_H(r_{p_i p_j})|$ is a totally symmetric pseudo-hydrogen wave function and $|\Phi(r_{p_k})|$ is a totally antisymmetric Slater wave function.

For the full three-quark system a similar wave function would apply. This does not necessarily mean that this wave function would lead to nuclear binding, but, given the order of magnitude of increase in the Q_2 well depth it would seem quite plausible that it might be a strong enough effect to produce a shallow well in the nuclear-binding-energy curve. A simple test would be to consider $SU_\ell(2)$ with just a string-flip potential, with α fixed, in which case scaling is restored and the Monte Carlo becomes quite straightforward to do.

When the $SU_\ell(2)$ flux-bubble model with moving colour was considered, the results showed that the Q_2 system dissociated into one light and one heavy meson. However, this model is not physical: rather we should consider the heavy quarks as a composite of two light quarks and use $SU_c(3)$ instead, so that a flux-tube cannot form between the two heavy quarks. For this “composite” model, the $\lambda_{p_i p_j}$ ’s of potential Eq. 13 become

$$\lambda_{p_i p_j} = \begin{cases} \frac{1}{3} & \text{if } p_i p_j \in \{bb, \bar{B}\bar{B}\} \\ \frac{1}{6} & \text{if } p_i p_j \in \{b\bar{G}, \bar{B}g\} \\ -\frac{1}{6} & \text{if } p_i p_j \in \{b\bar{B}, g\bar{G}\} \\ -\frac{1}{3} & \text{if } p_i p_j \in \{bg, \bar{B}\bar{G}\} \\ -\frac{4}{3} & \text{if } p_i p_j \in \min\{q_r \bar{q}_s\} \end{cases}, \quad (34)$$

such that $rg \sim \bar{B}$ and $rb \sim \bar{G}$ for the composite states, $bb \sim gg$ and $\bar{B}\bar{B} \sim \bar{G}\bar{G}$.

If the heavy quarks are considered to be a composite of two light u quarks then the effective mass would be about 600 MeV, which is a little too small to produce binding in this model, but for masses this low the adiabatic approximation would no longer be valid. Therefore, an interesting possibility would be to consider a many-body $SU_\ell(2)$ or $SU_\ell(3)$ flux-bubble model in which there is an imbalance between the quark and anti-quark masses. An interesting side effect of the improved wave-function is that it will automatically produce nucleon deformations, which, it has been argued, produce the contact interactions responsible for nuclear binding [19].

Further enhancements are expected by going to the full qqq nucleon model, followed by including flux-bubble interactions. In particular, the colour-hyperfine interaction which is shown by linked cluster expansion models to play a significant role in nuclear processes [17]. The flux-bubble model proved quite successful at combining colour-Coulomb interactions with flux-tube interactions. Although these interactions had very little effect on the Q_2 system, it was useful in demonstrating that extending the flux-tube model to include local perturbative QCD interactions can be done. This is important, since the nuclear hard-core potential is usually believed to have its origin in hyperfine interactions [2,5,17]. Therefore, it would prove most interesting to investigate the effect of adding more perturbative interactions to the Q_2 system. It also appears that relativistic effects are unimportant. With the addition of $SU_c(3)$ this would lead to a more realistic model of mesonic molecules which perhaps could be tested in the laboratory.

The Q_2 system has proven to be a very useful aid for trying to sort out the complexities of model building for nuclear matter. The details of the mechanics, from wave functions to dynamics to practical computing methods, of the flux-bubble model have now been thoroughly investigated. It appears that the flux-bubble model may prove to be very successful, not only for modeling nuclear matter but also for modeling mesonic molecules as well.

Acknowledgments

This work was supported by NSERC. The Monte Carlo calculations were performed on an 8 node DEC 5240 UNIX CPU farm, using Berkeley Sockets (TCP/IP) [20]. The computing facilities were provided by the Carleton University Department of Physics, OPAL, CRPP, and THEORY groups. We would like to thank M.A. Doncheski, H. Blundell, M. Jones, and J.S. Wright for useful discussions.

Appendix A. Analysis

This appendix contains a summary of the analysis done for the models given in sections 3.2 through 4 of this paper.

All of the results of these sections make use of the general potential Eq. 15. For $\bar{U}(R)$, as defined by Eq. 7, some analytical results were obtainable where the Q_2 system effectively dissociates into two isolated meson systems. For all of the plots this occurs at $\bar{U}(\infty)$, and for the linear and linear-plus-Coulomb plots this also occurs at $\bar{U}(0)$. In these regions, the analytic expression is given by (*cf.* [4])

$$E_{free} = 2 \left[\frac{g_T(\alpha)}{2\mu} \beta^2 + \sigma \left(\frac{g_L(\alpha, \beta)}{\beta} - g_0(\alpha, \beta) r_0 \right) - \frac{3}{4} \alpha_s \left(g_C(\alpha, \beta) \beta - \frac{(1 - g_0(\alpha, \beta))}{r_0} \right) \right], \quad (\text{A.1})$$

where

$$g_L(\alpha, \beta) = [1 - P(4/\alpha, 2(\beta r_0)^\alpha)] g_L(\alpha), \quad (\text{A.2})$$

$$g_C(\alpha, \beta) = P(2/\alpha, 2(\beta r_0)^\alpha) g_C(\alpha), \quad (\text{A.3})$$

$$g_0(\alpha, \beta) = 1 - P(3/\alpha, 2(\beta r_0)^\alpha), \quad (\text{A.4})$$

such that

$$g_T(\alpha) = \frac{\alpha^2 2^{\frac{2}{\alpha}} - 2}{\Gamma(3/\alpha)} \Gamma(2 + 1/\alpha), \quad (\text{A.5})$$

$$g_L(\alpha) = \frac{\Gamma(4/\alpha)}{2^{\frac{1}{\alpha}} \Gamma(3/\alpha)}, \quad (\text{A.6})$$

$$g_C(\alpha) = \frac{\Gamma(2/\alpha)}{2^{-\frac{1}{\alpha}} \Gamma(3/\alpha)}, \quad (\text{A.7})$$

$P(a, z) = 1 - \Gamma(a, z)/\Gamma(a)$, and $\Gamma(a, z)$ is the incomplete gamma function [21,22]. In the limits as $r_0 \rightarrow 0$ and $r_0 \rightarrow \infty$ Eq. (A.1) reduces to solutions for the purely linear,

$$E_{free} \underset{r_0 \rightarrow 0}{\rightarrow} 2 \left(\frac{g_T(\alpha)}{2\mu} \beta^2 + g_L(\alpha) \frac{\sigma}{\beta} \right), \quad (\text{A.8})$$

and purely Coulomb,

$$E_{free} \underset{r_0 \rightarrow \infty}{\rightarrow} 2 \left(\frac{g_T(\alpha)}{2\mu} \beta^2 - \frac{3}{4} \alpha_s g_C(\alpha) \beta \right), \quad (\text{A.9})$$

cases, respectively. Table A.1 gives a summary of the Monte Carlo vs. analytic results. The results for the linear and linear-plus-Coulomb potentials,

Table A.1
Monte Carlo (MC) vs. analytic results for Figs. 6, 7, 8 and 9.

Method		Fig.	R (fm)	E_{free} (MeV)	α	β (fm $^{-1}$)
Analytic	Eq. A.8	n.a.	0/ ∞	1709.61	1.75	1.37
MC	Linear	6	0	1709.424 \pm 0.038	1.74	1.37
			5	1709.492 \pm 0.044	1.72	1.38
	Coulomb	8	0	1709.647 \pm 0.032	1.77	1.36
			5	1709.485 \pm 0.032	1.75	1.36
Analytic	Eq. A.1	n.a.	0/ ∞	1527.07	1.74	1.37
MC	Linear	6	0	1527.171 \pm 0.029	1.78	1.36
			5	1527.171 \pm 0.029	1.78	1.36
	Coulomb	8	0	1527.884 \pm 0.041	1.74	1.34
			5	1527.884 \pm 0.041	1.74	1.34
MC	Flux-Bubble	6	5	1526.974 \pm 0.032	1.74	1.36
		7	5	1527.884 \pm 0.041	1.74	1.34
		8	5	1527.884 \pm 0.041	1.74	1.34
		9	5	1527.173 \pm 0.062	1.68	1.40

at $R = 0$ fm and $R = 5$ fm (*i.e.*, $\approx \infty$), were checked against Eqs. A.8 and A.1, respectively. The flux-bubble case, at $R = 5$ fm, was verified using Eq. A.1. The minima of the analytic expressions, which were used to verify the aforementioned models, were found *via* the `FindMinimum[...]` routine in Mathematica [21].

The binding energy of the Q_2 system can be estimated by doing a local parabolic fit [12] about the minimum of $\bar{U}(R)$: *i.e.*, by fitting

$$y(r) = \mathcal{C}(r - r_0)^2 - \mathcal{D} \quad (\text{A.10})$$

such that $\mathcal{C} = \mu_Q \omega^2 / [2(\hbar c)^2]$, where μ_Q is the reduced mass of the heavy

quarks. Therefore, the binding energy is simply

$$E_h^\nu = (\nu + \frac{1}{2})\hbar\omega - \mathcal{D}, \quad (\text{A.11})$$

which implies

$$\mu_Q \geq \mu_{\min} \equiv \frac{\mathcal{C}(\hbar c)^2}{2\mathcal{D}^2} \quad (\text{A.12})$$

in order to obtain binding. Table A.2 shows the results for the parabolic fits to the $\bar{U}(R)$'s in Fig. 6.

Table A.2

Results for local parabolic fitting about the minima of the plots in Figs. 6 and 8.

Model	Fig.	$\mathcal{C} (MeV/fm^2)$	$r_0 (fm)$	$\mathcal{D} (MeV)$	$\mu_{\min} (GeV)$
Linear	6	29.8 ± 1.5	0.4174 ± 0.0056	3.268 ± 0.058	54.3 ± 3.3
	8	234.8 ± 8.0	0.5288 ± 0.0057	82.55 ± 0.49	671 ± 24
Linear + Coulomb	6	28.7 ± 1.4	0.4134 ± 0.0045	3.098 ± 0.060	58.2 ± 3.6
	8	230.3 ± 8.0	0.5833 ± 0.0058	82.60 ± 0.49	657 ± 24
Flux-Bubble	6	20.0 ± 1.0	0.4614 ± 0.0034	2.783 ± 0.042	50.3 ± 2.9
	8	226.8 ± 8.0	0.5840 ± 0.0059	82.24 ± 0.49	653 ± 24

The asymptotic parts of the $\bar{U}(R)$'s were fitted to a Yukawa potential of the form

$$V_Y(r) = -2f^2 \frac{e^{-\mu r}}{r}. \quad (\text{A.13})$$

Table A.3 summarizes the Yukawa fits for all of the models.

Table A.3

Results for asymptotic Yukawa fits of the plots in Figs. 6, 8, and 9, where $m_{\text{ex}} = \hbar c \mu$.

Model	Fig.	$f^2 (\text{MeV fm})$	$\mu (\text{fm}^{-1})$	$m_{\text{ex}} (\text{MeV})$
Linear	6	2.49 ± 0.20	3.23 ± 0.21	637 ± 41
	8	27.3 ± 2.7	2.97 ± 0.16	586 ± 32
Linear+Coulomb	6	2.0 ± 2.2	3.0 ± 3.5	590 ± 690
	8	25.9 ± 2.7	2.89 ± 0.16	570 ± 32
Flux-Bubble	6	1.8 ± 2.3	2.4 ± 3.5	470 ± 690
	8	25.9 ± 2.7	2.89 ± 0.16	570 ± 32
	9	30.3 ± 2.1	3.10 ± 0.11	612 ± 32

References

- [1] G. Peter Lepage, *The Fall and Rise of Lattice QCD*, seminar at the Ottawa-Carleton Institute for Physics, Feb. 5th 1996.
- [2] M.M. Boyce and P.J.S. Watson, Nuc. Phys. **A580** (1994) 500.
- [3] C.J. Horowitz and J. Piekarewicz, Nucl. Phys. **A536** (1991) 669-696.
- [4] P.J.S. Watson, Nucl. Phys. **A494** (1989) 543.
- [5] M.M. Boyce, **String Inspired QCD and E₆ Models**, *Ph.D. thesis (1996)*, Carleton U., Dept. of Physics, 1125 Colonel By Dr., Ottawa, ONT, Canada, K1S-5B6; hep-ph/9609433.
- [6] J. Carlson, J. Kogut, and V.R. Pandharipna, Phys. Rev. **D27** (1983) 233.
- [7] M.M. Boyce and P.J.S. Watson, **SU(3) String-Flip Potential Models and Nuclear Matter**, “*MRST '94*,” conference, “*What Next? Exploring the Future of High-Energy Physics*,” Ed: J.R. Cudell, K.R. Dienes, and B. Margolis, World Scientific (1994); hep-ph/9501397.
- [8] John Weinstein and Nathan Isgur, Phys. Rev. **D41** (1990) 2236.
ibid, Phys. Rev. **D27** (1983) 588.
ibid, Phys. Rev. Lett. (1982) 659.
- [9] Leonard I. Schiff, **Quantum Mechanics**, 2nded, McGraw Hill (1968).
- [10] N. Metropolis, A.W. Rosenbluth, M.N. Rosenbluth, A.H. Teller, and E. Teller, J. Chem. Phys. **21** (1953) 1087.
- [11] M.M. Boyce, **The Distributed Minimization Algorithm**, *in preparation*.

- [12] Siegfried Flügge, **Practical Quantum Mechanics I**, Springer-Verlag, Berlin, Heidelbedrg, New York (1971).
- [13] B.H. Bransden and C.J. Joachain, **Physics of Atoms and Molecules**, Longman Group Limited (1983).
- [14] F. Gursey, *Nuovo Cimento* **7** (1958) 411.
W. Pauli, *Nuovo Cimento* **6** (1957) 205.
- [15] W. Heitler and F. London, *Z. Physik* **44** (1927) 455.
- [16] D. Ceperley, G.V. Chester, and M.H. Kalos, *Phys. Rev.* **B16** (1977) 3081.
- [17] Mohammad Nzar and Pervez Hoodbhoy, *Phys. Rev.* **C42** (1990) 1778.
- [18] D. Liberman, J.T. Waber and Don T. Cormer, *Phys. Rev.* **A27** (1986) 137.
- [19] Philip J. Siemens and Aksel S. Jensen, **Elements of Nuclei**, Many-Body Physics with the Strong Interaction, *Lecture Notes and Supplements in Physics*, Addison-Wesley (1987).
- [20] W. Richard Stevens, **UNIX Network Programming**, PTR Prentice Hall (1990).
- [21] Stephen Wolfram (*Wolfram Reasearch, inc: into@wri.com*), **Mathematica, A System for Doing Mathematics by Computer**, 2nd ed, Addison-Wesley (1991).
- [22] Milton Abramowitz and Irene A. Stegun, **Handbook of Mathematical Functions, with Formulas, Graphs, and Mathematical Tables**, Dover Publications Inc., New York (1972).